Antimony Dispersion and Phase Evolution in the Sb_2O_3−Fe_2O_3 System

Yan Huang*

College of Chemistry and Chemical Engineering, Nanjing University of Technology, Nanjing 210009, China

Patricio Ruiz

Unite de Catalyse et Chimie des Matériaux Divisés, Université Catholique de Louvain, B-1348, Louvain-la-Neuve, Belgium

Received: July 10, 2005; In Final Form: September 21, 2005

This paper studies the antimony spreading and segregation that occurred along with the oxidation and solid-state reactions in the Fe_2O_3−Sb_2O_3 system. XRD, SEM, TG-DSC and particularly XPS were employed for characterizations. Sb_2O_4 and $FeSbO_4$ are the only new phases detected. The formation of $FeSbO_4$ is a more exothermic but slower reaction than oxidation of Sb_2O_3. A mechanical grinding of Sb_2O_3 and Fe_2O_3 leads to a significant dispersion of Sb_2O_3 possibly because of its low hardness. Dispersion of reference Sb_2O_4 in this way is negligible. During the heating of a mixture of Sb_2O_3 and Fe_2O_3 with an atomic ratio of Sb/Fe = 0.5 at 200−1000 °C in ambient air, the thermal spreading of Sb_2O_3 onto Fe_2O_3 increases with increasing temperature until Sb_2O_3 is oxidized into Sb_2O_4. The surface atomic ratio of Sb/Fe measured by XPS, $R_{Sb/Fe}$, reaches a maximum around 400 °C. The complete oxidation of Sb_2O_3 leads to a decrease in $R_{Sb/Fe}$ because of poorer dispersibility of Sb_2O_4. The formation of $FeSbO_4$ starting at ca. 800 °C causes a further decrease in $R_{Sb/Fe}$, but the $R_{Sb/Fe}$ is still 3.2 times the nominal bulk Sb/Fe ratio when the Sb_2O_4 is completely transformed into $FeSbO_4$.

Introduction

Solid-state reaction under heat treatment is a conventional way to prepare compounds, typically mixed oxides and ceramics. Before reaction occurs, one solid may spread onto another through their contact boundaries—this phenomenon is called "thermal spreading", "spontaneous spreading", or "solid−solid wetting".[1−8] Generally, the surface of a solid will become "liquidlike" at its Tammann temperature, T_{Tam}, which is close to half of its melting point (absolute temperature), i.e., $T_{Tam} \approx 0.5T_{mp}$ (in K), and the thermal spreading is therefore often considered to occur at T_{Tam}. When the rate of thermal spreading is faster than that of the solid-state reaction, the nucleation of the new compound will start over the whole surface of the stationary solid, and gradually encapsulate it.[6] Thermal spreading can be an effective technique in the preparation of supported catalysts if the active components have relatively low T_{Tam}, such as MoO_3, V_2O_5, WO_3, etc. Our recent papers studied the antimony-rich surface layer through thermal spreading of Sb_2O_3 on Fe_2O_3.[9,10]

Antimony-containing mixed oxides such as Fe−Sb−O have been widely used as catalysts for selective oxidation and ammoxidation reactions.[11−15] The active component of the Fe−Sb−O catalyst has been well accepted to be $FeSbO_4$, and it can be prepared with Fe_2O_3 and antimony oxide. Several researchers studied the reactivity and phase evolution of the Fe_2O_3−Sb_2O_3 system heated in oxidizing atmosphere at different temperatures,[16−19] but the information about antimony spreading and segregation during the phase evolution has not been provided, and it has to be studied through surface characterizations. Moreover, the surface studies are extremely important for antimony-containing mixed oxides, because the antimony surface enrichment is almost a common feature, and essential for catalytic performances.[20−26] This paper studies in detail the thermal spreading of antimony along with the phase evolution upon heating a mixture of Sb_2O_3 and Fe_2O_3 in the air, and XPS measurements were particularly applied to investigate the changes in sample surface layer.

Experimental Section

A mixture of Fe_2O_3 (Fluka, 99.98%) and Sb_2O_3 (Fluka, 99.9%) with Sb/Fe = 0.5 was mixed by a mechanical grinding. For sufficient mixing, some acetone was added to help the grindings. After being dried at 100 °C overnight, the mixture was divided into several parts for calcination at different temperatures. The calcination was done at a rate of 1.5 °C/min up to the target temperature, which was then maintained for 5 h. The resulting samples were noted as Fe2Sb-200, Fe2Sb-300, Fe2Sb-400, Fe2Sb-500, Fe2Sb-600, Fe2Sb-700, Fe2Sb-800, Fe2Sb-900, and Fe2Sb-1000, with calcining temperatures of 200, 300, 400, 500, 600, 700, 800, 900, and 1000 °C, respectively.

The precursor mixture of Sb_2O_3 and Fe_2O_3 after drying at 100 °C was noted as Fe2Sb-100. For reference to Fe2Sb-100, a mixture of Sb_2O_4 (instead of Sb_2O_3) and Fe_2O_3 with the same Sb/Fe ratio was prepared by mechanical grinding with the same method, and it was noted as Fe2Sb-100#. Here, the Sb_2O_4 material was prepared through a calcination of Sb_2O_3 at 600 °C for 5 h in air. The surface areas of all the samples involved in this work are listed in Table 1.

The specific surface areas were measured with a Micromeritics ASAP 2000 system, using nitrogen adsorption at liquid nitrogen temperature. Powder XRD analysis was conducted on a Siemens D500 diffractometer with Cu Kα radiation operating at 40 kV and 30 mA. The simultaneous thermal analyses of TG (thermogravimetry) and DSC (differential scanning calo-

* Address correspondence to this author. E-mail: huangy@njut.edu.cn. Phone: +86-25-83587503. Fax: +86-25-83365813.

10.1021/jp053785+ CCC: $30.25
Published on Web 10/26/2005

TABLE 1: Results of Phase Analysis, Surface Area, and XPS

					binding energy (eV)		
sample	phases detected by XRD	area, m^2/g	$R_{Sb/Fe}$[a]	$R_{O/Fe}$[b]	Sb $3d_{3/2}$	Fe $2p_{3/2}$	O 1s
Fe2Sb-100#	Sb_2O_4, Fe_2O_3	4.5	0.40	-	539.8	710.5	530.0
Fe2Sb-100	Sb_2O_3, Fe_2O_3	5.0	1.9	5.4	539.7	710.6	530.5
Fe2Sb-200	Sb_2O_3, Fe_2O_3	5.1	1.6	4.2	539.8	710.8	530.3
Fe2Sb-300	Sb_2O_3, Fe_2O_3	4.8	10	15	539.7	710.5	530.5
Fe2Sb-400	Sb_2O_3, Fe_2O_3	4.3	43	56	539.8	710.8	530.5
Fe2Sb-500	Sb_2O_4, Fe_2O_3	4.1	20	41	539.8	711.1	530.7
Fe2Sb-600	Sb_2O_4, Fe_2O_3	3.8	18	36	539.6	710.6	530.2
Fe2Sb-700	Sb_2O_4, Fe_2O_3	3.4	16	34	540.0	711.0	530.6
Fe2Sb-800	$FeSbO_4$, Sb_2O_4, Fe_2O_3	2.5	10	21	539.8	711.2	530.5
Fe2Sb-900	$FeSbO_4$, Sb_2O_4, Fe_2O_3	1.9	4.8	12	539.8	711.2	530.9
Fe2Sb-1000	$FeSbO_4$, Fe_2O_3	1.3	1.6	5.9	539.9	710.9	530.2

[a] $R_{Sb/Fe}$: atomic ratio of Sb/Fe measured by XPS. [b] $R_{O/Fe}$: atomic ratio of O/Fe measured by XPS.

rimetry) were conducted on a NETSCH thermal analyzer STA 409 PG, using alumina as a reference. The analyzing sample was Fe2Sb-100 with a weight of 55.3 mg, which was heated from room temperature up to 1250 °C at a rate of 10 °C/min under a gas stream of $N_2/O_2 = 15/25$. SEM characterizations were carried out on a Philips XL40 scanning electron microscope. XPS analyses were performed on an SSI X-Probe (SSX-100 model 206) X-ray photoelectron spectrometer from FISONS with monochromatized and microfocused Al Kα radiation (1486.6 eV). The residual pressure in the analysis chamber was about 10^{-6} Pa. The irradiated zone was an elliptic spot with a shorter axis of 1000 μm, and the spot area was around 1.4 mm^2. The constant pass energy in the hemispherical analyzer was 150 eV. The binding energy scale was calibrated with the Au $4f_{7/2}$ peak fixed at 83.98 eV,[27] and the energy resolution determined by the full width at half-maximum (fwhm) of the Au $4f_{7/2}$ peak of a standard gold sample was about 1.6 eV. The angle between the direction of electron collection and the normal to the sample surface was 55°. The flood gun energy was set to 10 eV with a fine meshed nickel grid placed 3 mm above the sample surface. The spectra of survey spectrum C 1s, Sb 3d (together with overlapped O 1s), and Fe 2p were recorded subsequently, and finally the C 1s spectrum was recorded again to check the stability of charge compensation. The binding energies were referenced to the 1s peak of adventitious carbon bound only to carbon and hydrogen at 284.8 eV. After a Shirley-type background subtraction to minimize the background effect,[28] the spectra were decomposed with a Gaussian/Lorentzian percent function of 85%/15%. The XPS intensities were calculated by using atomic sensitivity factors provided by the spectrometer manufacturer. Peak areas of Fe 2p (including $Fe2p_{1/2}$, $Fe2p_{3/2}$, and their shake-up peaks), Sb $3d_{3/2}$, and O1s bands were used to quantify Fe, Sb, and O.

Results and Discussion

XRD patterns of all the samples are shown in Figure 1. Only two phases can be observed in Fe2Sb-100#: hematite Fe_2O_3 and cervantite Sb_2O_4. The phases in Fe2Sb-100 are Fe_2O_3 and senarmontite Sb_2O_3. In addition, a small amount of the valentinite type of Sb_2O_3 also can be recognized by a weak peak at $2\theta = 28.4°$ according to JCPDS 11-0689. It might come as an impurity from the resource senarmontite Sb_2O_3. The association of senarmontite (cubic) with its dimorphous valentinite (orthorhombic) is possibly due to the fact that both of them are oxidation products of stibnite (i.e., antimony sulfide). Few differences can be observed between the Fe2Sb-100 pattern and that of Fe2Sb-200, Fe2Sb-300, or Fe2Sb-400. The signals of both senarmontite and valentinite Sb_2O_3 phases completely disappear in the Fe2Sb-500 pattern, but new peaks appear which

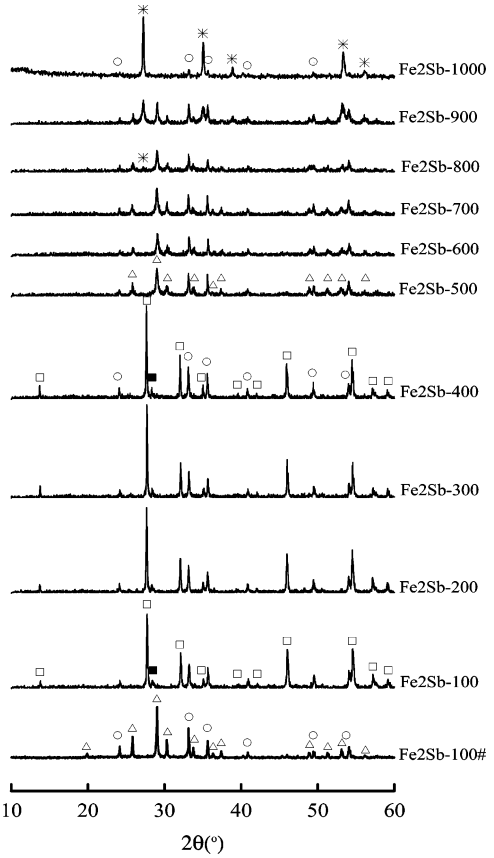

Figure 1. XRD patterns of Fe2Sb samples: □, senarmontite Sb_2O_3; ■ ,valentinite Sb_2O_3; △, Sb_2O_4; ○, Fe_2O_3; ∗, $FeSbO_4$.

can be assigned to cervantite Sb_2O_4. XRD patterns of Fe2Sb-600, Fe2Sb-700, and Fe2Sb-800 are almost the same as that of Fe2Sb-500. Apart from the signals of Fe_2O_3 and Sb_2O_4, all the other peaks in the Fe2Sb-900 pattern can be assigned to the squawcreekite $FeSbO_4$ according to JCPDS 34-0372. The Fe2Sb-1000 pattern reveals only phases of $FeSbO_4$ and Fe_2O_3, and the signals of Sb_2O_4 have completely disappeared. Since the peak at $2\theta = 27.2°$ has been confirmed to be the characteristic signal of $FeSbO_4$, and such a weak peak can be observed in the Fe2Sb-800 pattern, it can be concluded that a small amount of $FeSbO_4$ already has been formed in Fe2Sb-800. The results of the XRD phase analysis are summarized in Table 1. Except for Sb_2O_4 and $FeSbO_4$, no other new compounds are observed such as Fe_3O_4, Sb_2O_5, Sb_6O_{13}, $Fe_2Sb_2O_6$,[29] $Fe_2Sb_2O_7$,[30,31] $FeSb_2O_4$,[32] and so on. The situation will be the same even though the original ratio of Sb_2O_3/Fe_2O_3 is changed.[17,33] The involved reactions are

$$2Sb_2O_3 + O_2 \rightarrow 2Sb_2O_4 \quad (1)$$

$$2Fe_2O_3 + 2Sb_2O_4 + O_2 \rightarrow 4FeSbO_4 \quad (2)$$

Both of the above reactions are exothermic, and the absorption of oxygen will lead to a weight gain. Therefore, TG (thermogravimetry) and DSC (differential scanning calorimetry) would be suitable techniques to study those reactions. The results are exhibited in Figure 2. The TG diagram reveals that a slight decrease of weight occurs until about 400 °C—this is due to the loss of adsorbed acetone or moisture. Then, the sample weight begins to increase, and the increase at 450−520 °C is extremely quick. The weight gain slows down until ca. 720 °C then speeds up. A second sharp increase occurs at 900−1020 °C, then the weight becomes constant at 1040−1120 °C, but a decrease can be clearly observed afterward. In general, the TG diagram between 400 and 1100 °C can be separated at $T =$ 720 °C into two S-shaped zones, corresponding to weight gains of 2.3% and 2.2%, respectively. As confirmed by XRD results, they obviously can be associated with the above two oxidation reactions. Perfect consistence can be observed on the DSC diagram, where two exothermic peaks centered at 493 and 983 °C are clearly seen. According to reaction 1 and reaction 2, the two weight gains will be 2.62% and 2.55%, respectively, which are close to theoretical values.

The DSC diagram in Figure 2 also indicates that the exothermic peak at 493 °C is narrow but the second exothermic peak at 983 °C is very broad, which coincides with the TG results that the first weight gain is more rapid than the second, indicating that reaction 1 is more sensitive to temperature elevation. In addition, the area of the first DSC exothermic peak is 123 J/g, smaller than that of the second peak 183 J/g, indicating that reaction 1 released less heat than reaction 2. The loss of weight which begins at 1120 °C should be attributed to the decomposition of $FeSbO_4$, which releases both oxygen and volatile Sb_2O_3 following the reverse directions of reaction 2 and reaction 1.[16−17]

XPS responses of all the samples can be assigned to elements Fe, Sb, O, and the adventitious C, and no other elements have been detected. Figure 3 exhibits the Sb 3d and Fe 2p spectra of Fe2Sb-100 and Fe2Sb-100#. Although O 1s is overlapped by Sb $3d_{5/2}$, the latter can be determined by the following rules: (1) The full width at half-maximum (fwhm) of Sb $3d_{5/2}$ is equal to that of Sb $3d_{3/2}$. (2) Their distance is 9.34 eV. (3) The area of Sb $3d_{5/2}$ is theoretically 1.5 times that of Sb $3d_{3/2}$. According to the calculation in this way, any overestimation in area of $3d_{5/2}$ will cause an equivalent underestimation in area of O 1s, and vice versa. The atomic concentration C is proportional to the peak area A divided by the sensitivity factor F, i.e., $C \propto A/F$, and $F = 13.96$ for Sb $3d_{5/2}$ and $F = 2.50$ for O 1s. It can be calculated that any error in C_{Sb} will lead to 5.58 times that in C_O, therefore the precision of oxygen quantification in such a way is limited. As indicated in Figure 3, the O 1s of Fe2Sb-100 is a single peak around 530 eV, which can be assigned to O^{2-}, but Fe2Sb-100# reveals one more O 1s peak around 532 eV, which would be ascribed to the hydroxyl group.[34−36] It has been reported that the BE of Sb $3d_{3/2}$ in Sb_2O_3, Sb_2O_4, and Sb_2O_5 are 539.6, 539.8, and 540.2 eV, respectively.[37] Their differences are too small for XPS to distinguish antimony chemical states, thus quantities of Sb^{3+} and Sb^{5+} are summed together. As shown in Figure 3, the Fe 2p responses are typical signals of Fe^{3+}, which binding energy is around 711 eV.[38−39] Three couples of components are set to fit the Fe 2p band under the following rules: (1) The area of each $2p_{3/2}$ component is two times that of the coupled $2p_{1/2}$ component. (2) Fwhms of each couple of the components are the same. (3) The distance between each couple is 13.2 eV.[40] The quantification of iron is done with the overall area of Fe 2p (including $Fe2p_{1/2}$, $Fe2p_{3/2}$, and their shake-up peaks).

It can be observed in Figure 3 that the antimony response of Fe2Sb-100 is significantly stronger than that of Fe2Sb-100#, while the iron response of Fe2Sb-100 is significantly weaker than that of Fe2Sb-100#. Table 1 indicates that the $R_{Sb/Fe}$ of Fe2Sb-100# is 0.40, which is close to its nominal bulk Sb/Fe ratio. However, $R_{Sb/Fe}$ of Fe2Sb-100 is 1.9, which is as high as 3.8 times that of the nominal bulk Sb/Fe ratio. According to the preparation conditions of Fe2Sb-100, such an extraordinary dispersion of Sb_2O_3 should be caused by mechanical grinding. A similar result has been reported by Pillep et al.,[8] who compared the mechanical dispersion of antimony oxides on anatase TiO_2 by planetary ball milling. Moreover, they found that the effect of dispersion of Sb_2O_3 by wet milling (with water) for 1 h was comparable to that by dry milling for 20 h, and assigned this phenomenon to the formation of hydroxylated oxo species of Sb_2O_3 in the presence of water. In our work, acetone instead of water has been used, which should not lead to the formation of such species. Actually, it is rather popular that the effect of wet grinding or milling is better than dry no mater what kind of liquid is added. Then the question is still open why Sb_2O_3 can be significantly dispersed by grinding or milling and Sb_2O_4 cannot. Usually, a softer solid will be easier to grind. The mineral hardnesses (Mohs') of senarmontite Sb_2O_3, cervantite Sb_2O_4, and hematite Fe_2O_3 are 2.3, 4.5, and 6, respectively,[41] indicating Sb_2O_3 is the softest and Sb_2O_3 is nearly as soft as graphite (hardness: 1−2). Hence, Sb_2O_3 can be pulverized easily and dispersed onto Fe_2O_3.

Figure 4 exhibits the Fe2p and Sb 3d spectra of the 10 samples from Fe2Sb-100 to Fe2Sb-1000, with final heating temperatures of 100−1000 °C. With the increase in heating temperature, the intensity of Sb $3d_{3/2}$ tends to increase, and after a maximum at 400 °C, it tends to decrease. The intensity of Fe 2p changes in the reverse direction. The measured atomic ratios of Sb/Fe and O/Fe are listed in Table 1, and specially, Figure 5 plots $R_{Sb/Fe}$ against heating temperature. It can be found that the $R_{Sb/Fe}$ changes little at 200 °C, but it increases from 1.6 sharply up to 10 at 300 °C and up to 34 at 400 °C. TG-DTA and XRD results indicate that the oxidation of Sb_2O_3 was not detected bellow this temperature. Such a rapid increase in $R_{Sb/Fe}$ is consistent with our previous report that the thermal spreading of Sb_2O_3 can occur at a temperature well below that needed for oxidation because the Tammann temperature, T_{Tam}, of Sb_2O_3 is only about 200 °C.[9] During this period, the increase in $R_{Sb/Fe}$ can be attributed to the thermal spreading of Sb_2O_3 driven by the increasing temperature.

It is interesting that the $R_{Sb/Fe}$ decreases sharply at 500 °C. Accordingly, the Sb_2O_3 has been completely oxidized into Sb_2O_4. On one hand, the thermal spreading of Sb_2O_3 is not sustainable anymore, but the thermal spreading of Sb_2O_4 is still difficult at this temperature.[8,9] On the other hand, thermal spreading is also called "solid−solid wetting", i.e., Sb_2O_3 can be dispersed homogeneously onto Fe_2O_3 via the "wetting" effect; this is the reason $R_{Sb/Fe}$ for Fe2Sb-400 reaches as high as 68 times the nominal bulk Sb/Fe ratio. Once Sb_2O_3 is oxidized, the Sb_2O_4 layer on Fe_2O_3 will not maintain so high dispersibility without such a "wetting" effect, therefore Sb_2O_4 may aggregate or partially leave the Fe_2O_3 surface, leading to a decrease in $R_{Sb/Fe}$.

Figure 5 reveals that the $R_{Sb/Fe}$ further decreases at 600 and 700 °C. Although the thermal spreading of Sb_2O_4 has to be

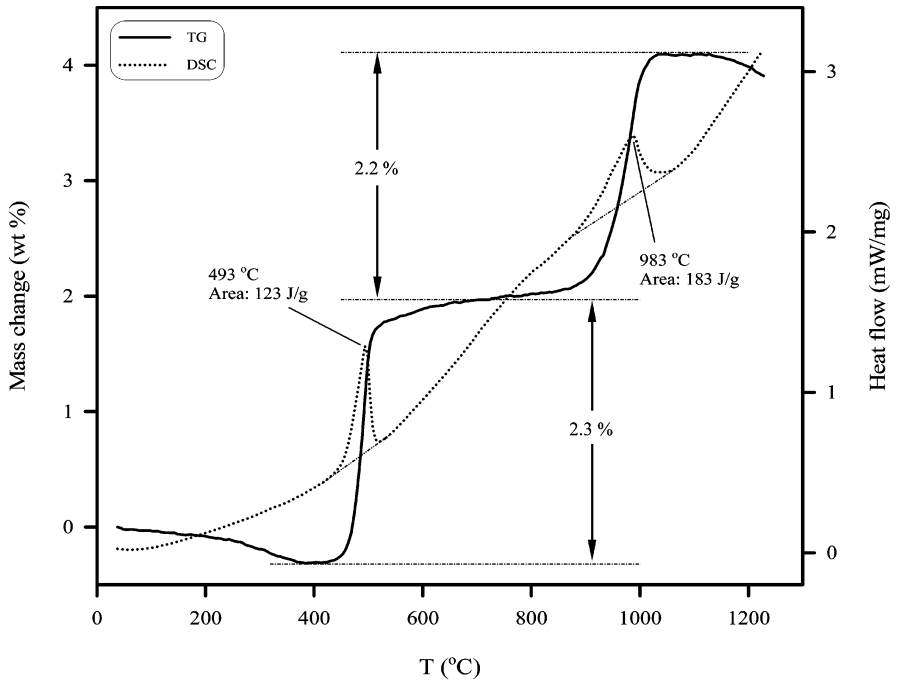

Figure 2. TG-DSC analyses on a mixture of Sb_2O_3 and Fe_2O_3 with Sb/Fe = 0.5.

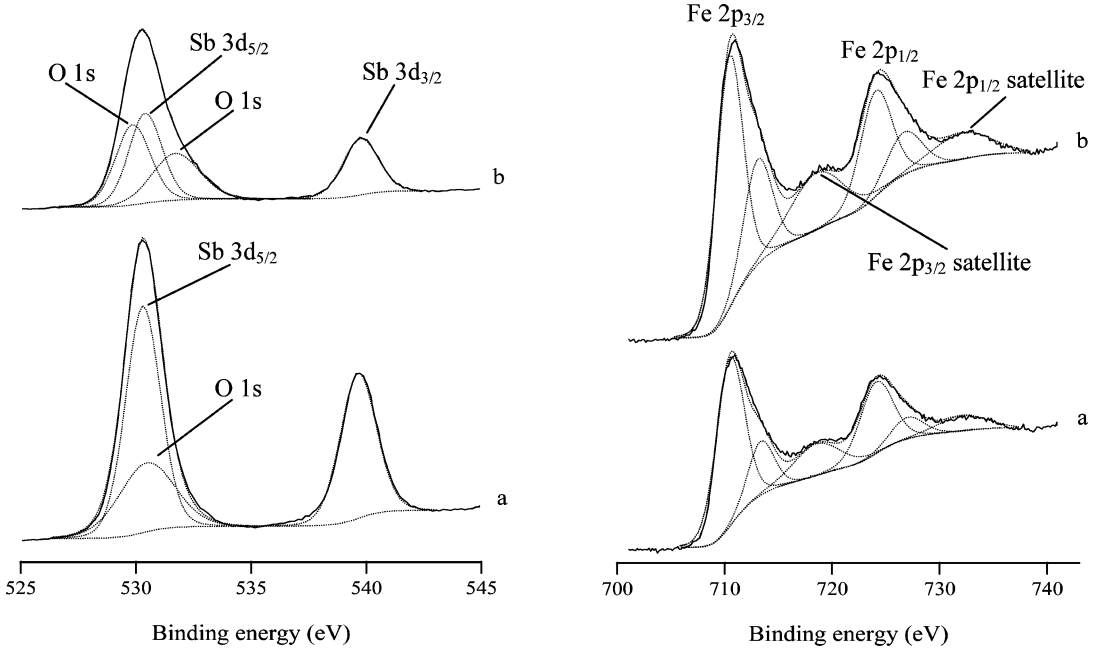

Figure 3. Fe 2p and Sb 3d XPS spectra of (a) Fe2Sb-100 and (b) Fe2Sb-100#.

taken into account at the increasing temperature, this still has not become a dominant factor. It can be seen that $R_{Sb/Fe}$ decreases more quickly at 800 °C; accordingly, XRD and TG-DTA results indicate that Sb_2O_4 starts to react with Fe_2O_3 into $FeSbO_4$ at this temperature. The further decrease in $R_{Sb/Fe}$ at 900 and 1000 °C can be ascribed to the further formation of $FeSbO_4$ until Sb_2O_4 is completely run out. It should be noted that the $R_{Sb/Fe}$ of Fe2Sb-1000 is still as high as 1.6, which is 3.2 times that of the nominal bulk Sb/Fe ratio. Since Fe2Sb-1000 is a mixture of $FeSbO_4$ and Fe_2O_3, the $R_{Sb/Fe}$ would have been <1 if only these two species were taken into account. Recently, we studied the antimony segregation in the $FeSbO_4-Fe_2O_3$ system, and found that Fe_2O_3 grains are encapsulated by a layer of $FeSbO_4$, while the $FeSb_2O_6$ species exist on the $FeSbO_4$ surface.[33]

SEM micrographs of Fe2Sb-100#, Fe2Sb-100, Fe2Sb-400, Fe2Sb-600, Fe2Sb-800, and Fe2Sb-1000 are shown in Figure 6. Fe2Sb-100# is a mixture of Sb_2O_4 and Fe_2O_3, and Figure 6a indicates two kinds of particles. As confirmed by EDS analysis, the big crystals are Sb_2O_4 and the small particles are Fe_2O_3. Similarly, the Sb_2O_3 crystals can be distinguished from Fe_2O_3 particles in Fe2Sb-100. The crystals of Sb_2O_3 have straight edges while Sb_2O_4 crystals look very irregular. Comparing Figure 6a with Figure 6b reveals that an agglomeration of Fe_2O_3 grains occurred in Fe2Sb-100. This is consistent with the finding in Figure 3, and the agglomeration should be caused by the very fine particles of Sb_2O_3 during mechanical grinding. Fe2Sb-400 has the same phases as Fe2Sb-100, but Figure 6c indicates that many clumps of powder aggregates have been formed. Similarly, Fe2Sb-600 has the same phases as Fe2Sb-100#, but a great

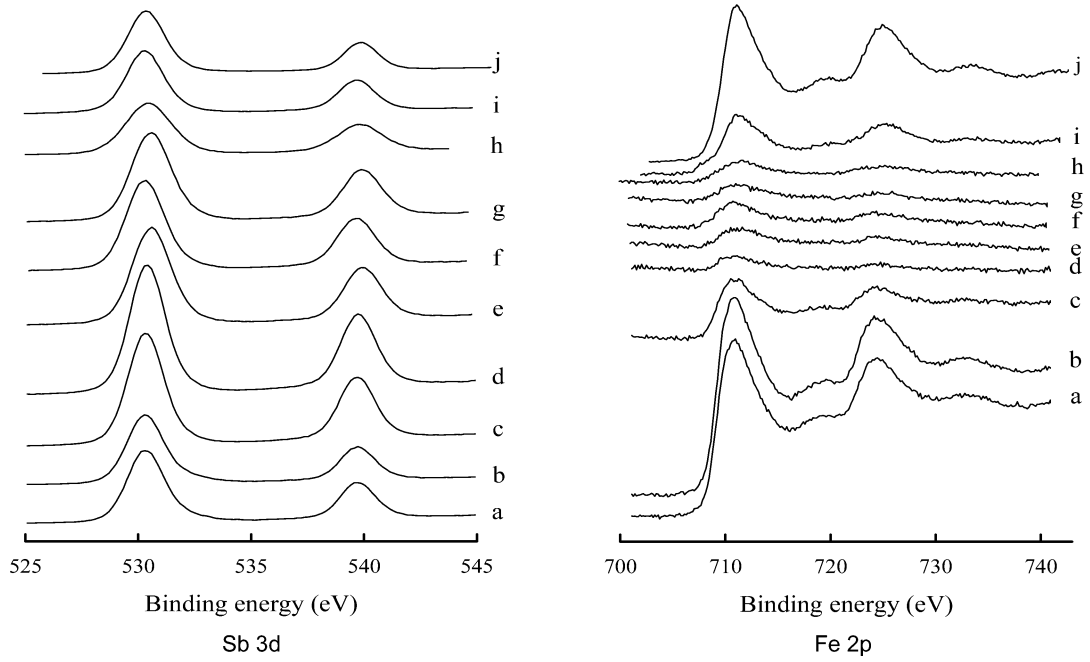

Figure 4. Fe 2p and Sb 3d XPS spectra of (a) Fe2Sb-100, (b) Fe2Sb-200, (c) Fe2Sb-300, (d) Fe2Sb-400, (e) Fe2Sb-500, (f) Fe2Sb-600, (g) Fe2Sb-700, (h) Fe2Sb-800, (i) Fe2Sb-900, and (j) Fe2Sb-1000.

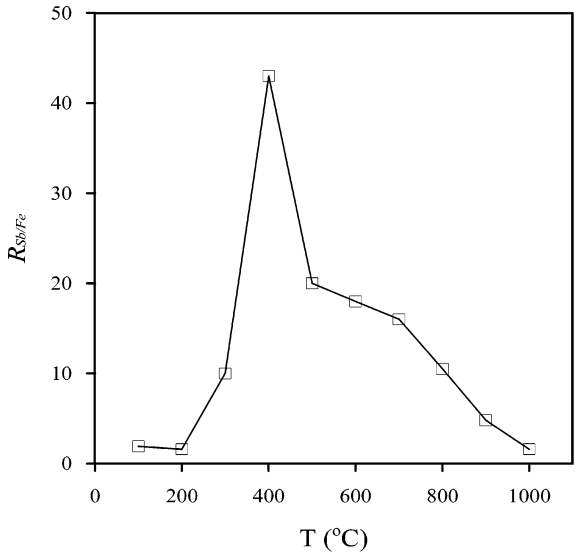

Figure 5. Effect of heating temperature on the surface atomic ratio of Sb/Fe, $R_{Sb/Fe}$.

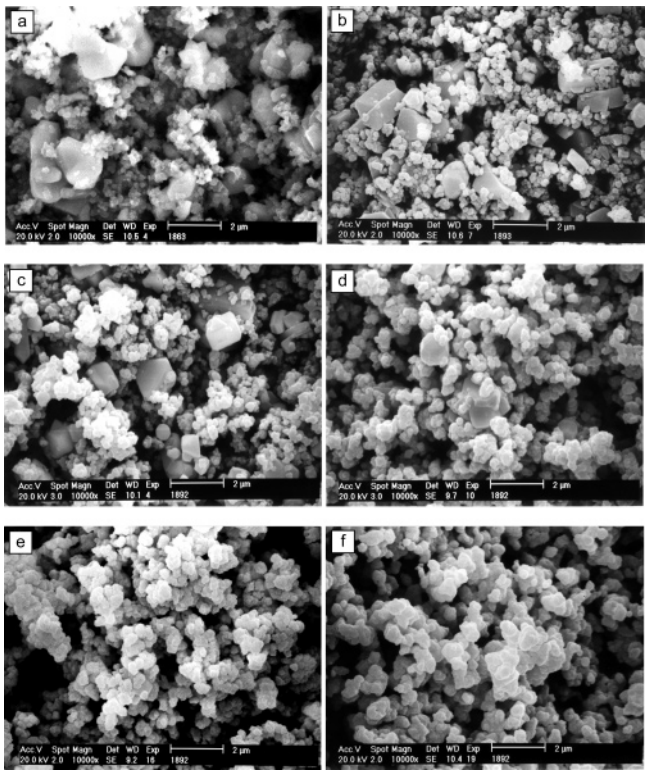

Figure 6. SEM micrographs of (a) Fe2Sb-100#, (b) Fe2Sb-100, (c) Fe2Sb-400, (d) Fe2Sb-600, (e) Fe2Sb-800, and (f) Fe2Sb-1000.

difference can be observed between Figure 6a and Figure 6d. The average particle size increases and the number of independent Sb_2O_4 crystals decreases. More severe aggregation feature can be seen in Fe2Sb-800 by Figure 6e, and no independent Sb_2O_4 crystals can be recognized, indicating that Sb_2O_4 and Fe_2O_3 have been severely sintered, and XRD and TG-DSC results indicate that $FeSbO_4$ has been formed. Figure 6f exhibits a hard aggregation feature, and the particles in Fe2Sb-1000 look smoother.

Conclusion

Sb_2O_4 and $FeSbO_4$ are the only new phases detected in the $Fe_2O_3-Sb_2O_3$ system (atomic ratio of Sb/Fe = 0.5) heated in the air. The formation of $FeSbO_4$ is a more exothermic but slower reaction than oxidation of Sb_2O_3. Mechanical grinding of Sb_2O_3 with Fe_2O_3 leads to a significant dispersion of Sb_2O_3 possibly because of its low hardness. The thermal spreading of Sb_2O_3 onto Fe_2O_3 increases with the increasing temperature until Sb_2O_3 is oxidized then it decreases. The surface concentration of antimony further decreases due to the formation of $FeSbO_4$, but a segregation of antimony still remains when the Sb_2O_4 is completely transformed into $FeSbO_4$.

Acknowledgment. We thank Dr. M. Genet, Unité de Catalyse et Chimie des Matériaux Divisés, Université Catholique de Louvain, Belgium, for assistance in XPS experiments. Financial support from the Natural Science Foundation of

Jiangsu Province, China, under Grant No. BK2005113 is gratefully acknowledged.

References and Notes

(1) Honicke, D.; Xu, J. *J. Phys. Chem.* **1988**, *92*, 301.
(2) Haber, J.; Machej, T.; Servicka, E.; Wachs, I. *Catal. Lett.* **1995**, *32*, 101.
(3) Xie, Y.; Tang, Y. *Adv. Catal.* **1990**, *37*, 1.
(4) Xie, Y.; Zhu, Y.; Zhao, B.; Tang, Y. *Stud. Surf. Sci. Catal.* **1998**, *118*, 441.
(5) Jentoft, F.; Schmelz, H.; Knözinger, H. *Appl. Catal.* **1997**, *161*, 167.
(6) Knözinger, H.; Taglauer, E. In *Catalysis*; Spivey, J. J., Agarwal, S. K., Eds.; The Royal Society of Chemistry: Cambridge, UK, 1993; Vol. 10, p 1.
(7) Leyrer, J.; Margraf, R.; Taglauer, E.; Knözinger, H. *Surf. Sci.* **1988**, *201*, 603.
(8) Pillep, B.; Behrens, P.; Schubert, U.; Spengler, J.; Knözinger, H. *J. Phys. Chem. B* **1999**, *103*, 9595.
(9) Huang, Y.; Wang, G.; Valenzuela, R.; Cortés-Corberán, V. *Appl. Surf. Sci.* **2003**, *210*, 346.
(10) Huang, Y.; Wang, G.; Cortés-Corberán, V. *Surf. Sci.* **2003**, *547*, 55.
(11) Carrazán, S.; Cadus, L.; Dieu, P.; Ruiz, P.; Delmon, B. *Catal. Today* **1996**, *32*, 311.
(12) Castillo, R.; Dewaele, K.; Ruiz, P.; Delmon, B. *Appl. Catal.* **1997**, *153*, L1.
(13) Fattore, V.; Fuhran, Z.; Manara, G.; Notari, B. *J. Catal.* **1975**, *37*, 223.
(14) van Steen, E.; Schnobel, M.; Walsh, R.; Riedel, T. *Appl. Catal.* **1997**, *165*, 349.
(15) Magagula, Z.; Van Steen, E. *Catal. Today* **1999**, *49*, 155.
(16) Martinelli, A.; Ferretti, M.; Buscaglia, V.; Cabella, R.; Lucchetti, G. *J. Therm. Anal. Calorim.* **2002**, *70*, 123.
(17) Walczak, J.; Felipek, E.; Bosacka, M. *Solid State Ionics* **1997**, *103*, 1363.
(18) Zhang, T.; Zhang, R.; Zhang, J.; Li, Y.; Hing, P. *J. Mater. Res.* **2000**, *15*, 2356.
(19) Zhang, T.; Hing, P. *J. Mater. Sci.* **1990**, *10*, 509.
(20) Sala, F.; Trifiró, F. *J. Catal.* **1976**, *41*, 1.
(21) Aso, I.; Furukawa, S.; Yamazoe, N.; Seiyama, T. *J. Catal.* **1980**, *64*, 29.
(22) Bowker, M.; Bicknell, C.; Kervin, P. *Appl. Catal.* **1996**, *136*, 205.
(23) Allen, M. D.; Poulston, S.; Bithell, E.; Goringe, M. J.; Bowker, M. *J. Catal.* **1996**, *163*, 204.
(24) Carbucicchio, M.; Centi, G.; Trifirò, F. *J. Catal.* **1985**, *91*, 85.
(25) Teller, R.; Brazdil, J.; Grasselli, R. *J. Chem. Soc., Faraday Trans. 1* **1985**, *81*, 1693.
(26) Straguzzi, G.; Bischoff, K.; Koch, T.; Schuit, G. C. A. *J. Catal.* **1987**, *104*, 47.
(27) Seah, M. P. *Surf. Interface Anal.* **1989**, *14*, 488.
(28) Shirley, D. A. *Phys. Rev. B* **1972**, *5*, 4709.
(29) Mason, B.; Vitaliano, C. J. *Min. Mag.* **1953**, *30*, 100.
(30) Berlepschi, P.; Armbruster, T.; Brugger, J.; Criddles, A. J.; Graeser, S. *Min. Mag.* **2003**, *67*, 31.
(31) Hussak, E.; Prior, G. T. *Min. Mag.* **1897**, *11*, 302.
(32) Benaichouba, B.; Bussiere, P.; Friedt, J.; Sancchez, J. *Appl. Catal.* **1983**, *8*, 237.
(33) Huang, Y.; Ruiz, P. The Nature of Antimony-enriched Surface Layer of Fe−Sb Mixed Oxides. *Appl. Surf. Sci.*, in press.
(34) Zhao, L. Z.; Young, V. *J. Electron Spectrosc. Relat. Phenom.* **1984**, *34*, 45.
(35) Wagner, C. D.; Passoja, D. E.; Hillery, H. F.; Kinisky, T. G.; Six, H. A.; Jansen, W. T.; Taylor, J. A. *J. Vac. Sci. Technol.* **1982**, *21*, 933.
(36) Shuttleworth, D. *J. Phys. Chem.* **1980**, *84*, 1629.
(37) Delobel, R.; Baussart, H.; Leroy, J.; Grimblot, J.; Gengembre, L. *J. Chem. Soc., Faraday Trans. 1* **1983**, *79*, 879.
(38) Paparazzo, E. *J. Electron Spectrosc. Relat. Phenom.* **1987**, *43*, 97.
(39) Kim, K. J.; Moon, D. W.; Lee, S. K.; Jung, K. H. *Thin Solid Films* **2000**, *360*, 118.
(40) Allen, G. C.; Curtis, M. T.; Hooper, A. J.; Tucker, P. M. *J. Chem. Soc., Dalton Trans.* **1974**, 1525.
(41) Lide, D. R., Ed. *CRC Handbook of Chemistry and Physics*, 85th ed.; CRC Press: Boca Raton, FL, 2005; p 4-151.